MNRAS **000**, 000–000 (0000) Preprint March 3, 2024 Compiled using MNRAS LATEX style file v3.0

Large Covariance Matrices: Smooth Models from the 2-Point Correlation Function

Ross O'Connell[1], Daniel Eisenstein[2], Mariana Vargas[3], Shirley Ho[1], Nikhil Padmanabhan[4]
[1] *McWilliams Center for Cosmology, Carnegie Mellon University, 5000 Forbes Ave, Pittsburgh, PA 15213, USA*
[2] *Harvard-Smithsonian Center for Astrophysics, 60 Garden St., Cambridge, MA 02138, USA*
[3] *Instituto de Física, Universidad Nacional Autónoma de México, Apdo. Postal 20-364, México*
[4] *Dept. of Physics, Yale University, New Haven, CT, 06511, USA*

March 3, 2024

ABSTRACT

We introduce a new method for estimating the covariance matrix for the galaxy correlation function in surveys of large-scale structure. Our method combines simple theoretical results with a realistic characterization of the survey to dramatically reduce noise in the covariance matrix. For example, with an investment of only $\approx 1,000$ CPU hours we can produce a model covariance matrix with noise levels that would otherwise require $\sim 35,000$ mocks. Non-Gaussian contributions to the model are calibrated against mock catalogs, after which the model covariance is found to be in impressive agreement with the mock covariance matrix. Since calibration of this method requires fewer mocks than brute force approaches, we believe that it could dramatically reduce the number of mocks required to analyse future surveys.

1 INTRODUCTION

Covariance matrix estimation is a fundamental challenge in precision cosmology. In the standard approach many artificial or "mock" catalogs are created that mimic the properties of the cosmological data set, the analysis is performed on each mock catalog, and a sample covariance computed using those results. From a certain point of view this approach is very simple, since the mock catalogs are statistically independent from one another. The potential stumbling block is that the sample covariance provides a noisy estimate of the true covariance, and covariance matrix noise can degrade the final measurement. Reducing noise in the covariance matrix to acceptable levels generally requires a large number of mock catalogs, and covariance matrix estimation can consume the majority of computational resources for current analyses. Moreover, there is a clear trade-off between the number of mock catalogs required and the accuracy of any individual mock. We aim to improve this situation with a new method for covariance matrix estimation that combines simple theoretical results with a realistic characterization of the survey, and that can be calibrated against a relatively small number of mocks. We will demonstrate that this approach produces a covariance matrix suitable for analysis of baryon acoustic oscillations (BAO) in modern surveys.

The consequences of covariance matrix noise have been a subject of recent interest (Taylor et al. 2013; Dodelson & Schneider 2013; Percival et al. 2014). It is generally true that when cosmological parameters are determined from an observable estimated in $N_{\rm bins}$ (for example a correlation function or power spectrum), and the corresponding covariance matrix is estimated using $N_{\rm mocks}$ mock catalogs, then there is a fractional increase in the uncertainty in the cosmological parameters, relative to an ideal measurement, of $\mathcal{O}\left(1/\left(N_{\rm mocks} - N_{\rm bins}\right)\right)$. In other words, having $N_{\rm mocks} \sim 10 \times N_{\rm bins}$ (rather than much larger) has an impact on the final parameter estimates comparable to reducing the volume of a survey by $\sim 10\%$. When the covariance matrix is estimated using a sample covariance of mock catalogs, there is thus an incentive to make $N_{\rm mocks} - N_{\rm bins}$ as large as possible.

While some current surveys have achieved $N_{\rm mocks} \sim 100 \times N_{\rm bins}$, we are concerned that this may not be achievable in future surveys. First, we expect that many future analyses will attempt to utilize more accurate mocks, for example incorporating realistic light cones, and that this will raise the computational cost of a single

mock. In addition, many future surveys (e.g. Euclid (Laureijs et al. 2011), DESI (Levi et al. 2013), WFIRST-AFTA (Spergel et al. 2015)) have proposed to perform tomographic analyses, rather than analysing a single redshift range; where current analyses might estimate the correlation function using 40 bins, a tomographic analysis using 10 redshift slices will necessarily use 400 bins. We emphasize that while available computing resources may increase at a pace that accommodates increasing mock requirements, there will always be an opportunity cost to producing large numbers of mocks – given fixed computing resources, reducing the number of mocks required by a factor of 100 means that the amount of computing time that can be spent on each mock increases by a factor of 100.

It is possible to address the problem by reducing $N_{\rm bins}$, rather than increasing $N_{\rm mocks}$. For example, current BAO analyses typically compress the angular dependence of the correlation function into two multipole moments or a small number of angular wedges, rather than retaining the full angular dependence of the correlation function. Proposals have also been made for an analogous compression of redshift-dependence for tomographic analyses (Zhu et al. 2015). While these approaches provide an intriguing complement to the method we will describe, we point out that there may be tension between the optimal modes for compressing the signal, and the characteristic modes associated with systematic effects. For example, reducing the angular dependence of the redshift space galaxy correlation function to monopole and quadrupole modes provides highly efficient compression of the underlying correlation function, but systematic effects tend to depend on line-of-sight or transverse separations between points and thus compress poorly into the monopole and quadrupole modes.

Motivated by these concerns, we propose a new method for covariance matrix estimation that accommodates large $N_{\rm bins}$ while requiring only a modest number of $N_{\rm mocks}$, and results in a dramatic reduction in noise in the covariance matrix relative to the sample covariance. In Section 2 we provide a simple analytic expression for the covariance matrix of a galaxy correlation function. This extends the results of Bernstein (Bernstein 1994) to incorporate position-dependent number densities and weights. In Section 3 we numerically integrate this expression over a realistic survey geometry, assuming that the underlying galaxy field is Gaussian. We find reasonable agreement between our results and a sample covariance computed from 1,000 quick particle mesh (QPM, (White et al. 2014)) mocks produced using the same survey geometry. In Section 4 we show that increasing the level of shot noise in the Gaussian model covariance matrix brings it closer to the full, non-Gaussian covariance matrix. After fitting the shot noise increase using the QPM mocks, we find exceptional agreement between our method and the QPM sample covariance.

2 N-POINT FUNCTIONS AND THE COVARIANCE MATRIX

The basic observation that motivates this work is that the covariance matrix of an n-point function can be written as a combination of $2n-$ and lower-point functions. As a simple example, consider the correlation function ξ_{ij} of a density field δ_i:

$$\xi_{ij} = \delta_i \delta_j \,. \tag{2.1}$$

The covariance between two observations of the correlation function is simply

$$\begin{aligned} {\rm cov}\left(\xi_{ij}, \xi_{k\ell}\right) &= \langle \xi_{ij}\xi_{kl}\rangle - \langle \xi_{ij}\rangle \langle \xi_{k\ell}\rangle & (2.2)\\ &= \langle \delta_i\delta_j\delta_k\delta_\ell\rangle - \langle \delta_i\delta_j\rangle \langle \delta_k\delta_\ell\rangle & (2.3)\\ &= \langle \xi_{ijk\ell}\rangle + \langle \xi_{ik}\rangle \langle \xi_{j\ell}\rangle + \langle \xi_{i\ell}\rangle \langle \xi_{jk}\rangle \,, & (2.4) \end{aligned}$$

where we have used $\xi_{ijk\ell}$ to denote the connected 4-point function. For fields that are Gaussian or nearly Gaussian, the value of expressions like (2.4) should be clear: they allow us to convert an estimate of the 2-point correlation function into an estimate of that correlation function's covariance matrix.

In the following we will demonstrate how to extend this simple result to correlation functions estimated in bins Θ^a_{ij}, how to modify it for a Poisson-sampled density field, and how to incorporate the inhomogeneous number density and non-uniform weighting that occur in realistic surveys. A more comprehensive derivation of these results, including finite-volume corrections (but without weights and assuming homogeneity), can be found in (Bernstein 1994). An earlier application of these ideas, with less attention to reproducing the detailed survey geometry, can be found in (Xu et al. 2013).

2.1 Poisson Sampling

Suppose that we have divided the volume of a galaxy survey into many cells, each small enough that it contains at most one galaxy. The overdensity in cell i is then

$$\delta_i = \frac{b_i}{n_i} - 1 \,, \tag{2.5}$$

where $b_i = 1$ if the cell contains a galaxy and $b_i = 0$ otherwise, and n_i is the expected number of galaxies in the cell (note that this may vary from cell to cell). Since the choice of cell size is arbitrary we can choose $n_i \ll 1$, and in this limit the overdensity satisfies a useful identity:

$$\delta_i^2 \approx \frac{1}{n_i}\left(1+\delta_i\right). \tag{2.6}$$

This identity encodes our intuitive understanding of Poisson sampling, which is that at sufficiently short separations $\left(\delta_i\delta_j \to \delta_i^2\right)$ the correlation function is replaced by shot noise ($\sim 1/n_i$).

We estimate the correlation function as

$$\hat{\xi}^a = (RR^a)^{-1}\sum_{i\neq j}\Theta^a_{ij}n_in_j\delta_i\delta_j\,, \tag{2.7}$$

$$RR^a \equiv \sum_{i\neq j}\Theta^a_{ij}n_in_j\,. \tag{2.8}$$

The binning matrices Θ^a_{ij} are one for pairs of points i,j that fall in bin a, and zero otherwise. We assume that the bins require finite separation, so that both sums run over *distinct* points i,j. Note that RR^a coincides with the usual notion of RR pair counts. The covariance of $\hat{\xi}^a$ is then

$$\left\langle\hat{\xi}^a\hat{\xi}^b\right\rangle - \left\langle\hat{\xi}^a\right\rangle\left\langle\hat{\xi}^b\right\rangle = \left(RR^aRR^b\right)^{-1}\sum_{i\neq j,k\neq\ell}\Theta^a_{ij}\Theta^b_{k\ell}n_in_jn_kn_\ell\left[\langle\delta_i\delta_j\delta_k\delta_\ell\rangle - \langle\delta_i\delta_j\rangle\langle\delta_k\delta_\ell\rangle\right]. \tag{2.9}$$

To relate these quantities to the usual $n-$point functions, we must rewrite the sum in terms of non-coincident points,

$$\sum_{i\neq j,k\neq\ell}\Theta^a_{ij}\Theta^b_{k\ell}n_in_jn_kn_\ell\langle\delta_i\delta_j\delta_k\delta_\ell\rangle = \sum_{i\neq j\neq k\neq\ell}\Theta^a_{ij}\Theta^b_{k\ell}n_in_jn_kn_\ell\langle\delta_i\delta_j\delta_k\delta_\ell\rangle + S_{\rm single} + S_{\rm double}, \tag{2.10}$$

with $S_{\rm single}$ containing single contractions,

$$S_{\rm single} = \sum_{i\neq j\neq k}\Theta^a_{ij}\Theta^b_{ki}n_i^2n_jn_k\left\langle\delta_i^2\delta_j\delta_k\right\rangle \tag{2.11}$$

$$= \sum_{i\neq j\neq k}\Theta^a_{ij}\Theta^b_{ki}n_in_jn_k\left[\langle\delta_j\delta_k\rangle + \langle\delta_i\delta_j\delta_k\rangle\right], \tag{2.12}$$

and $S_{\rm double}$ containing double contractions,

$$S_{\rm double} = \delta^{ab}\sum_{i\neq j}\Theta^a_{ij}n_i^2n_j^2\left\langle\delta_i^2\delta_j^2\right\rangle \tag{2.13}$$

$$= \delta^{ab}\sum_{i\neq j}\Theta^a_{ij}n_in_j\left[1+\langle\delta_i\delta_j\rangle\right]. \tag{2.14}$$

We have used (2.6) to simplify these expressions, and δ^{ab} are Kronecker deltas. These contractions can be visualized with the diagrams in fig. 1.

After considering the possible contractions, we arrive at the following expression for C^{ab}, the model covariance matrix:

$$C^{ab} = C_4^{ab} + C_3^{ab} + C_2^{ab}\,, \tag{2.15}$$

$$C_4^{ab} \equiv \left(RR^aRR^b\right)^{-1}\sum_{i\neq j\neq k\neq\ell}\Theta^a_{ij}\Theta^b_{k\ell}n_in_jn_kn_\ell\left[\xi_{ijk\ell} + \xi_{ik}\xi_{j\ell} + \xi_{i\ell}\xi_{jk}\right], \tag{2.16}$$

$$C_3^{ab} \equiv 4\times\left(RR^aRR^b\right)^{-1}\sum_{i\neq j\neq k}\Theta^a_{ij}\Theta^b_{ki}n_in_jn_k\left[\xi_{ijk} + \xi_{jk}\right], \tag{2.17}$$

$$C_2^{ab} \equiv 2\times\delta_{ab}\left(RR^aRR^b\right)^{-1}\sum_{i\neq j}\Theta^a_{ij}n_in_j\left[\xi_{jk}+1\right], \tag{2.18}$$

where ξ_{ijk} and $\xi_{ijk\ell}$ denote the connected 3- and 4-point functions, respectively. A continuum limit yields

$$C_4^{ab} = \left(RR^aRR^b\right)^{-1}\int d^3\vec{r}_id^3\vec{r}_jd^3\vec{r}_kd^3\vec{r}_\ell\Theta^a\left(\vec{r}_i-\vec{r}_j\right)\Theta^b\left(\vec{r}_k-\vec{r}_\ell\right)n\left(\vec{r}_i\right)n\left(\vec{r}_j\right)n\left(\vec{r}_k\right)n\left(\vec{r}_\ell\right)$$
$$\times\left[\xi_4\left(\vec{r}_i,\vec{r}_j,\vec{r}_k,\vec{r}_\ell\right) + \xi\left(\vec{r}_i-\vec{r}_k\right)\xi\left(\vec{r}_j-\vec{r}_\ell\right) + \xi\left(\vec{r}_i-\vec{r}_\ell\right)\xi\left(\vec{r}_j-\vec{r}_k\right)\right], \tag{2.19}$$

$$C_3^{ab} = 4\times\left(RR^aRR^b\right)^{-1}\int d^3\vec{r}_id^3\vec{r}_jd^3\vec{r}_k\Theta^a\left(\vec{r}_i-\vec{r}_j\right)\Theta^b\left(\vec{r}_k-\vec{r}_i\right)n\left(\vec{r}_i\right)n\left(\vec{r}_j\right)n\left(\vec{r}_k\right)$$
$$\times\left[\xi_3\left(\vec{r}_i,\vec{r}_j,\vec{r}_k\right) + \xi\left(\vec{r}_i-\vec{r}_k\right)\right], \tag{2.20}$$

$$C_2^{ab} = 2\delta_{ab}\times\left(RR^aRR^b\right)^{-1}\int d^3\vec{r}_id^3\vec{r}_j\Theta^a\left(\vec{r}_i-\vec{r}_j\right)n\left(\vec{r}_i\right)n\left(\vec{r}_j\right)$$
$$\times\left[\xi\left(\vec{r}_i-\vec{r}_j\right)+1\right], \tag{2.21}$$

$$RR^a = \int d^3\vec{r}_id^3\vec{r}_j\Theta^a\left(\vec{r}_i-\vec{r}_j\right)n\left(\vec{r}_i\right)n\left(\vec{r}_j\right). \tag{2.22}$$

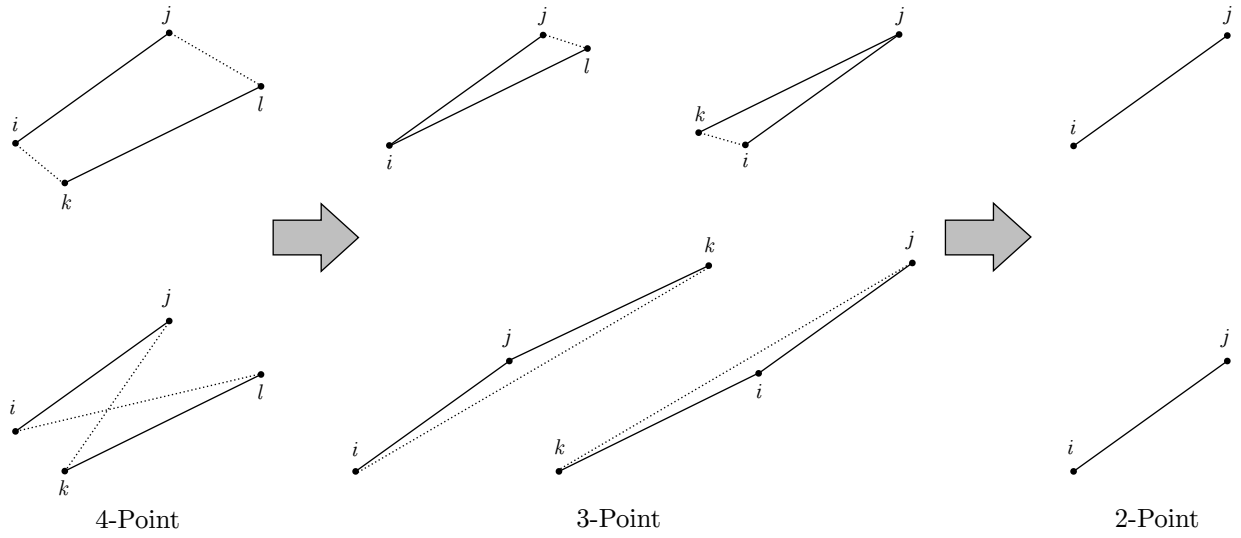

Figure 1. Configurations of points that contribute to the covariance matrix integrals. Starting from the two 4-point configurations that contribute to C_4, single contractions generate the four possible 3-point configurations of C_3, and double contractions generate the 2-point configuration of C_2. Solid lines indicate pairs of points that are governed by a binning function, $\Theta^a\left(\vec{r}_i-\vec{r}_j\right)$, while dotted lines indicate pairs of points that are governed by a factor of the correlation function, $\xi\left(\vec{r}_i-\vec{r}_k\right)$.

with ξ_3 and ξ_4 now denoting the connected 3- and 4-point functions and $n\left(\vec{r}\right)$ the expected number density at $\vec{r}$.

We can introduce a final complication, which is a non-uniform weighting scheme (e.g. FKP weights (Feldman et al. 1994)). The basic observation is that a factor of $w_i w_j$ is added to (2.7) and (2.8), leading to an additional factor of $w_i w_j w_k w_\ell$ in (2.9), but that (2.6) is unmodified. We therefore find

$$\begin{aligned} C_4^{ab} &= \left(RR^aRR^b\right)^{-1}\int d^3\vec{r}_i d^3\vec{r}_j d^3\vec{r}_k d^3\vec{r}_\ell \Theta^a\left(\vec{r}_i-\vec{r}_j\right)\Theta^b\left(\vec{r}_k-\vec{r}_\ell\right) \\ &\quad \times n\left(\vec{r}_i\right)n\left(\vec{r}_j\right)n\left(\vec{r}_k\right)n\left(\vec{r}_\ell\right)w\left(\vec{r}_i\right)w\left(\vec{r}_j\right)w\left(\vec{r}_k\right)w\left(\vec{r}_\ell\right) \quad (2.23) \\ &\quad \times\left[\xi_4\left(\vec{r}_i,\vec{r}_j,\vec{r}_k,\vec{r}_\ell\right)+\xi\left(\vec{r}_i-\vec{r}_k\right)\xi\left(\vec{r}_j-\vec{r}_\ell\right)+\xi\left(\vec{r}_i-\vec{r}_\ell\right)\xi\left(\vec{r}_j-\vec{r}_k\right)\right], \quad (2.24) \\ C_3^{ab} &= 4\times\left(RR^aRR^b\right)^{-1}\int d^3\vec{r}_i d^3\vec{r}_j d^3\vec{r}_k \Theta^a\left(\vec{r}_i-\vec{r}_j\right)\Theta^b\left(\vec{r}_k-\vec{r}_i\right)n\left(\vec{r}_i\right)n\left(\vec{r}_j\right)n\left(\vec{r}_k\right) \\ &\quad \times w^2\left(\vec{r}_i\right)w\left(\vec{r}_j\right)w\left(\vec{r}_k\right)\left[\xi_3\left(\vec{r}_i,\vec{r}_j,\vec{r}_k\right)+\xi\left(\vec{r}_i-\vec{r}_k\right)\right], \quad (2.25) \\ C_2^{ab} &= 2\delta_{ab}\times\left(RR^aRR^b\right)^{-1}\int d^3\vec{r}_i d^3\vec{r}_j \Theta^a\left(\vec{r}_i-\vec{r}_j\right)n\left(\vec{r}_i\right)n\left(\vec{r}_j\right) \\ &\quad \times w^2\left(\vec{r}_i\right)w^2\left(\vec{r}_j\right)\left[\xi\left(\vec{r}_i-\vec{r}_j\right)+1\right], \quad (2.26) \\ RR^a &= \int d^3\vec{r}_i d^3\vec{r}_j \Theta^a\left(\vec{r}_i-\vec{r}_j\right)n\left(\vec{r}_i\right)n\left(\vec{r}_j\right)w\left(\vec{r}_i\right)w\left(\vec{r}_j\right). \quad (2.27) \end{aligned}$$

C_2, C_3, and C_4 all scale as $1/\mathrm{Vol}$, and are independent of overall rescalings of the weights. They also exhibit a simple scaling with the number density

$$C_m^{ab}\propto n^{m-4}. \quad (2.28)$$

In sec. 3 we will numerically integrate the *Gaussian* terms in (2.24)-(2.26). Rather than attempt to integrate the *non-Gaussian* terms involving ξ_3 and ξ_4, in sec. 4 we will develop a simple method that uses increased shot noise to approximate the effects of non-Gaussianity.

3 INTEGRATING THE GAUSSIAN MODEL

In order to test the value of equations (2.24)-(2.27) for generating covariance matrices, we will attempt to reproduce the covariance matrix of a set of mock catalogs. Specifically, we will use 1,000 quick particle mesh (QPM) mocks (White et al. 2014) that mimic the CMASS sample of the Baryon Oscillation Spectroscopic Survey (BOSS). Redshift space distortions (RSD) are included, but no reconstruction algorithms [REFS] have been applied to these mocks.

We use a correlation function estimated in 35 radial bins of width $\delta r = 4\,h^{-1}$Mpc, covering $r = 40 - 180\,h^{-1}$Mpc, and 10 angular bins of width $\delta\mu = 0.1$, covering $\mu = 0-1$. This is more bins, by at least a factor of

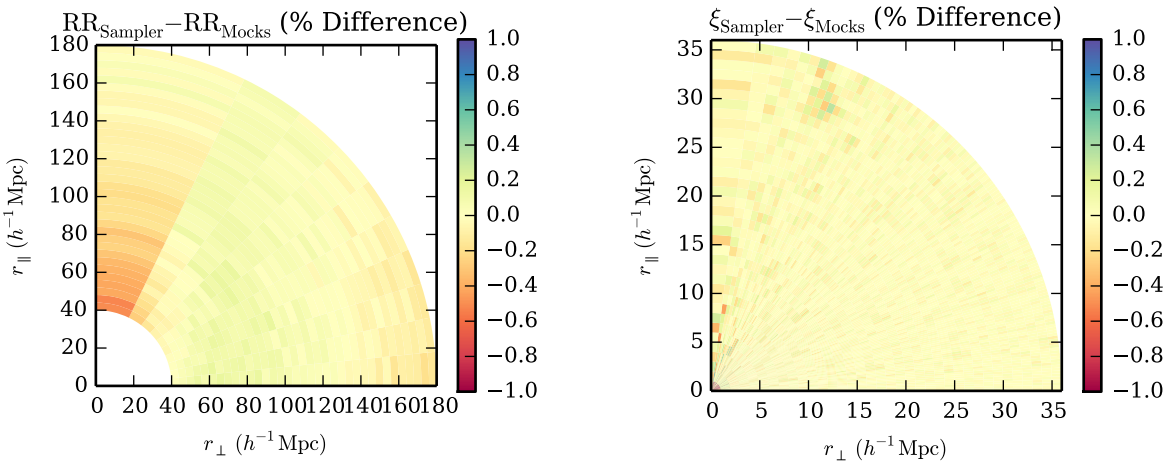

Figure 2. Using RR pair counts as a test of the survey geometry, we see that the representation of the survey in our sampler is in good agreement with the survey geometry in the mocks. We test the correlation function in our sampler by integrating it over the same bins used in the mocks, and find the two to be in excellent agreement.

5, than would be used in a typical multipole analysis of BAO in the galaxy correlation function. A more aggressive binning was chosen in part because it makes the covariance matrix problem more challenging and makes the noise in the sample covariance matrix more readily apparent.

The numerical integration is performed with a new software package[1], "Rascal: A Rapid Sampler for Large Covariance Matrices". It allows flexible specification of the cosmology, redshift distribution, and model correlation function, and can accept angular completeness masks in the MANGLE format (Swanson et al. 2008). The sampling algorithm is described below, in sec. 3.3.

3.1 Survey Geometry

The QPM mocks have a flat ΛCDM cosmology with $\Omega_m = 0.29$. The geometry of the mock catalogs can be decomposed into radial and angular components. In the radial direction, the redshift-dependent number density $\overline{n}(z)$ and weights $w(z)$ are calibrated to the QPM mocks. We set $\overline{n}(z) = 0$ outside of the redshift bounds of the CMASS sample, i.e. for $z < 0.43$ and $z > 0.7$. In the angular directions, the survey mask specifies the completeness of the survey, $c(\Omega)$. The number density at a point in the survey is thus given by

$$n(z, \Omega) = \overline{n}(z)\, c(\Omega)\,. \tag{3.1}$$

In order to compare our implementation of the survey geometry with that of the mock catalogs, we compare the values of RR^a that we compute with the values taken from the mock random catalogs. The results are shown in fig. 2. We find a small offset between our integration and the mocks which varies as a function of $r_\perp$. This arises because the mocks are generated using a "veto mask" which replicates holes in the survey smaller than the telescope field-of-view (e.g. areas obscured by bright stars). Querying this mask is quite time-consuming, and we have not used in when generating the samples in this paper.

3.2 Correlation Function

In order to integrate equations (2.24)-(2.26) we must specify a model correlation function (not to be confused with the estimated correlation function, whose covariance matrix we are computing). Rather than use the linear theory correlation function, or one derived from perturbation theory, we use the non-linear correlation function estimated from the 1,000 QPM mocks. This ensures that the correlation function we use for integration agrees at relatively short scales ($r \gtrsim 1\,h^{-1}$Mpc) with the mocks, faithfully reproducing non-linear features such as the "finger-of-God".

In the mocks, the correlation function is evaluated with radial bins that are $1\,h^{-1}$Mpc wide and 120 angular bins covering $\mu = 0 - 1$. A potential problem is that we then have estimates of the correlation function *averaged over* a bin, while the interpolation scheme used in our code assumes that the correlation function is specified *at the center* of the bin. In order to address this we adopted an iterative scheme. We first treated the bin-averaged

[1] An introduction to the package, as well as the python code, will be available at a later date.

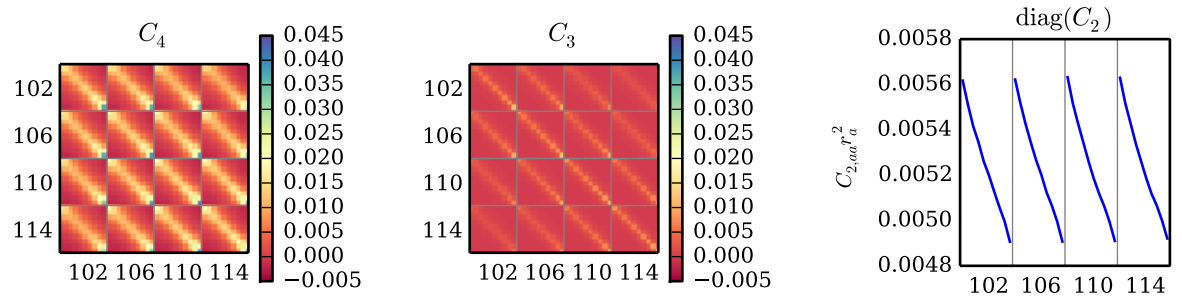

Figure 3. The three covariance matrix templates defined in (2.24)-(2.26), as evaluated using our sampler. The Gaussian covariance matrix is the sum of C_4, C_3, and the diagonal matrix C_2. We show only a small portion of the covariance matrix, but this is sufficient to illustrate the high degree of convergence achieved in $\sim 1,000$ CPU hours with our sampler.

values $\xi^m_{\rm mock}$ from the mocks as bin-center values, then performed the analogous bin-averaged integrals using our code,

$$\xi^m_{\rm out} = (RR^a)^{-1} \int d\vec{r}_i d\vec{r}_j \Theta^m\left(\vec{r}_i - \vec{r}_j\right) n\left(\vec{r}_i\right) w\left(\vec{r}_i\right) n\left(\vec{r}_j\right) w\left(\vec{r}_j\right) \xi_{in}\left(\vec{r}_i - \vec{r}_j\right). \tag{3.2}$$

We then rescaled the bin-centered input values of ξ according to $\xi^m_{\rm out}/\xi^m_{\rm mock}$ and repeated the procedure. After three iterations, we arrived at sub-percent agreement between our implementation of the correlation function, as measured by its bin-averages, and the correlation function in the mocks. This is demonstrated in fig. 2.

3.3 Importance Sampling

The integral (2.24) is 12-dimensional. It also has relatively limited support, so that the simplest Monte Carlo approaches converge quite slowly. We achieve acceptable convergence rates by using importance sampling. We begin by choosing a bin $\Theta^a\left(\vec{r}_i - \vec{r}_j\right)$, then generate uniform draws of the separation $\vec{r}_i - \vec{r}_j$ within that bin. We then draw $|\vec{r}_j - \vec{r}_k|$ and $|\vec{r}_i - \vec{r}_\ell|$ from a pdf proportional to $r^2\left|\xi_0\left(r\right)\right|$, where $\xi_0\left(r\right)$ is the spherically-averaged correlation function. The angular components of $\vec{r}_j - \vec{r}_k$ and $\vec{r}_i - \vec{r}_\ell$ are again determined by uniform draws. Finally, we sort the sets of four points according to which bin $\Theta^b\left(\vec{r}_k - \vec{r}_\ell\right)$ they fall in. We therefore are able to estimate one column of C_4^{ab} from a set of draws. Since the integration proceeds column-by-column, this approach is trivially parallelizable. Moreover, the same draws can be used to determine C_3^{ab} and C_2^{aa}.

In fig. 3 we show portions of the C_4, C_3, and C_2 that we computed using this method and the inputs described above. These runs were completed on a desktop computer, requiring $\approx 1,000$ CPU hours to complete. Although the noise in our samples is not Wishart distributed, we can characterize our results in terms of an effective number of mocks by choosing a range of bins where the precision matrix should be very close to zero, then measuring the noise in those bins. Inverse Wishart statistics would imply

$$\mathrm{var}\left(\Psi^{ab}\right) \approx \frac{\Psi^{aa}\Psi^{bb}}{N_{\rm mocks} - N_{\rm bins}} \tag{3.3}$$

for bins where $\Psi^{ab} \approx 0$. We therefore define the effective number of mocks as

$$N_{\rm eff} \equiv N_{\rm bins} + \left[\mathrm{var}\left(\frac{\Psi^{ab}}{\sqrt{\Psi^{aa}\Psi^{bb}}}\right)\right]^{-1}, \tag{3.4}$$

with the variance taken across bins with $\Psi^{ab} \approx 0$ from a single realization. Using bins with $r^a \geq 142\,h^{-1}$Mpc and $r^b \leq 82\,h^{-1}$Mpc, we find $N_{\rm eff} \sim 35,000$ for the C_4, C_3, and C_2 generated for this paper. The convergence of the sampler is easily characterized in terms of $N_{\rm eff}$, with a roughly linear relationship between CPU time used running the sampler and $N_{\rm eff}$.

3.4 Comparison with Mocks

We have constructed a simple Gaussian model for the covariance matrix, taking as inputs the survey geometry and non-linear correlation function. Given the modesty of these inputs and the simplicity of the Gaussian model, the close agreement between our model covariance matrix and the covariance matrix determined using 1,000 QPM mock catalogs with the same geometry and correlation function is remarkable. In figure 4 we plot a portion of the precision matrix as determined from the mocks, as computed in the Gaussian model, and the difference between the two. We observe discrepancies between the two at the $\sim 10\%$ level, most noticeable for diagonal entries in

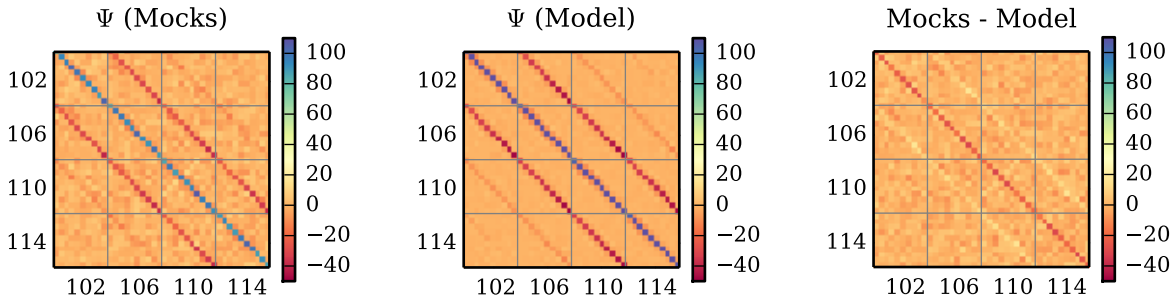

Figure 4. A small portion of the precision (inverse covariance) matrix, as determined from mock catalogs and from our Gaussian model (without fitting). The correlation function is evaluated in bins with $\delta r = 4\,h^{-1}$Mpc and $\delta\mu = 0.1$. In these plots bins are ordered first in r (covering $r = 102\,h^{-1}$Mpc to $r = 114\,h^{-1}$Mpc), then in μ ($\mu = 0$ to $\mu = 1$). The reduction in noise in the model precision matrix, relative to the mock precision matrix, is readily apparent. The residuals in the rightmost plot are surprisingly small, given that we are using the purely Gaussian model, but also indicate the need for non-Gaussian corrections to the model (see fig. 6).

the precision matrix and in entries for bins with the same μ that are adjacent in r, and we now investigate the consequences of these discrepancies.

There are two reasons for using the precision matrix rather than the covariance matrix in this comparison. First, the structure of the precision matrix is considerably simpler than the structure of the covariance matrix, as can be seen by comparing fig. 3 and fig. 4. Second, the precision matrix, rather than the covariance matrix, is what is used to compute χ^2 statistics, and thus is the quantity that is most relevant in analysis. Finally, we point out that large eigenvalues of the precision matrix correspond to small eigenvalues of the covariance matrix, and vice versa, so agreement between precision matrices cannot easily be established by comparing the corresponding covariance matrices directly.

We have chosen two approaches to a more detailed comparison of the precision matrices. In the first approach we begin by computing weighted residuals between the two precision matrices,

$$\mathrm{resid}^{ab} = \frac{\Psi^{ab}_{\mathrm{model}} - \Psi^{ab}_{\mathrm{mock}}}{r_a r_b}\,, \tag{3.5}$$

with the $r-$weighting chosen to remove the naive $r-$dependence of the precision matrix. We then compute for each bin

$$\Delta r^{ab} = r^a - r^b\,, \tag{3.6}$$

$$\Delta\mu^{ab} = \mu^a - \mu^b, \tag{3.7}$$

and average together the residuals for all bins with the same values of Δr and $\Delta\mu$. The result is shown in fig. 5, where it is clear that we observe significant discrepancies when $\Delta r = \Delta\mu = 0$ and when $\Delta r = 4\,h^{-1}$Mpc, $\Delta\mu = 0$. We also observe small residuals for bins with $\Delta r = 0\,h^{-1}$Mpc, $\Delta\mu = 0.1$, which were not readily apparent in figure 4.

While the first method of comparison provides a direct check on the precision matrix, at least for modest Δr and $\Delta\mu$, the second method uses a Fisher matrix to focus on modes of interest in BAO analyses. We assume a simple model for the correlation function,

$$\xi_{\mathrm{Fisher}}(r,\mu) = \xi_0(b,\beta,\alpha,\epsilon;r)\,P_0(\mu) + \xi_2(b,\beta,\alpha,\epsilon;r)\,P_2(\mu) + \sum_{i=0}^{2}\left(a_{0,i}r^{i-2}P_0(\mu) + a_{2,i}r^{i-2}P_2(\mu)\right). \tag{3.8}$$

This correlation function depends on ten parameters: the correlation function bias b, redshift-space distortion parameter β, isotropic BAO rescaling factor α, anisotropic BAO rescaling factor ϵ, and the six systematic parameters $a_{0,i}, a_{2,i}$. P_0 and P_2 are Legendre polynomials. We then use the usual Fisher matrix formula to relate the precision matrix for these parameters to the precision matrix for the correlation function:

$$\Psi^{ij}_{\mathrm{Parameters}} = \frac{\partial\xi^T_{\mathrm{Fisher}}}{\partial p_i}\Psi_\xi\frac{\partial\xi_{\mathrm{Fisher}}}{\partial p_j}\,, \tag{3.9}$$

with p_i running over the ten parameters. We invert $\Psi_{\mathrm{Parameters}}$ to find $C_{\mathrm{Parameters}}$, then marginalize over b, β, and the systematic parameters to find a covariance matrix for α and ϵ alone. The resulting error ellipses are shown in fig. 5, and the parameters that define those ellipses are show in table 2. Again, discrepancies are readily apparent, though we defer a quantitative discussion of those discrepancies for sec. 4.3.

It is telling that the discrepancies we observe between the mock and model precision matrices appear primarily on the diagonal of the precision matrix, and for bins that are adjacent to one another. Referring back to the integral in (2.24), we see that e.g. $|\vec{r}_i - \vec{r}_k|$ and $|\vec{r}_j - \vec{r}_\ell|$ can only reach very small values for overlapping or

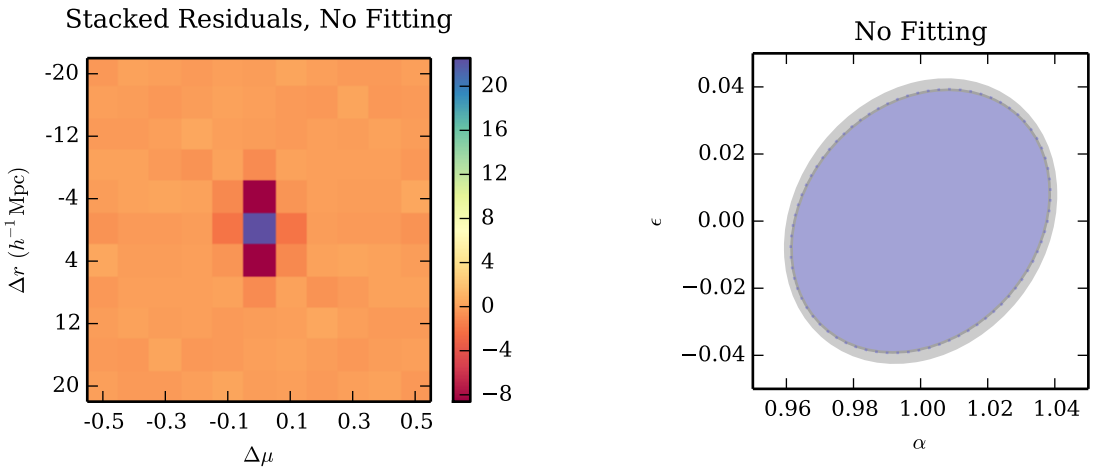

Figure 5. Comparison between the mock precision matrix and our (unfit) Gaussian model precision. Stacking the residuals reveals discrepancies on the diagonal of the precision matrix, and also for bins that share a μ range and are adjacent in r. Error ellipses for the BAO parameters α and ϵ show small discrepancies between the mocks (gray), model (blue), and noisy realizations of the model (dashed). The purely Gaussian model performs surprisingly well for BAO error estimation, but the discrepancies can be reduced with a non-Gaussian extension of the model (see fig. 9).

adjacent bins. We therefore interpret these discrepancies as a sign that our model is missing a contribution at short scales; since we know the 2-point correlation function at short scales very well, it seems most likely that the observed discrepancies are a consequence of dropping the non-Gaussian terms involving ξ_3 and ξ_4. In the following we will attempt to model the non-Gaussian contributions without building explicit models for ξ_3 and ξ_4.

4 A SIMPLE MODEL FOR NON-GAUSSIANITY

We now attempt to improve the the results of the previous section by introducing a one-parameter model to accommodate the effects of non-Gaussianity. Roughly speaking, we expect the connected 3- and 4-point functions to be large at small separations, then fall off rapidly at larger separations. A simple way of making the galaxy field "more correlated" at short scales is to increase the amount of shot noise. Recall from (2.28) that $C_m \propto n^{m-4}$, so that we can implement this rescaling using the integrals performed in the previous section:

$$C_{\rm NG}(a) = C_4 + aC_3 + a^2 C_2 \,. \tag{4.1}$$

As we will show, this simple rescaling yields a precision matrix that is in excellent agreement with the mock precision matrix. For applications of a similar model to the covariance of the power spectrum, see (Carron et al. 2014).

In the following we will develop two approaches for fitting $C_{\rm NG}$ to the mocks. While the two approaches have distinct advantages and disadvantages, they will lead to substantially similar error ellipses for the BAO parameters α and ϵ.

4.1 $\mathcal{L}_1$ Likelihood

If we consider the mock correlation functions as noisy draws from a distribution described by $\Psi_{\rm NG}(a) = C_{\rm NG}^{-1}(a)$, the likelihood for a is

$$\mathcal{L}_1(a) \quad = \quad \prod_{\alpha \in \text{mocks}} \sqrt{\frac{\det \Psi_{\rm NG}(a)}{(2\pi)^{N_{\rm bins}}}} \exp\left[-\frac{1}{2}\xi_\alpha^T \Psi_{\rm NG}(a)\,\xi_\alpha\right]. \tag{4.2}$$

With a bit of rearranging, this becomes

$$-\log \mathcal{L}_1(a) = \frac{N_{\rm mocks}}{2}\left[\mathrm{tr}\left(\Psi_{\rm NG}(a)\, C_{\rm mocks}\right) - \log\det \Psi_{\rm NG}(a)\right] + \dots \,, \tag{4.3}$$

where the omitted terms are independent of a. Given our expression (4.1) for the model covariance matrix and the mock covariance matrix, it is straightforward to find the maximum likelihood value for a. This fitting dramatically reduces the residuals between the model and mock precision matrices, as shown in fig. 8, and brings the mock and model $\alpha - \epsilon$ error ellipses into better agreement, as show in fig. 9.

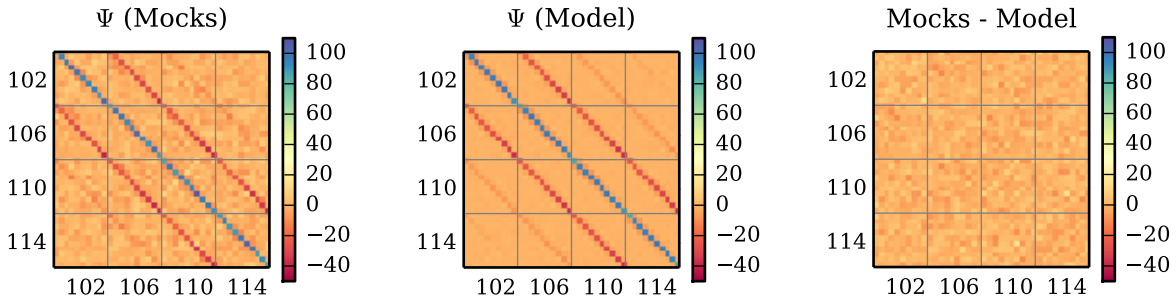

Figure 6. A small portion of the precision matrix, as determined from mock catalogs and from our non-Gaussian model (fit using the $\mathcal{L}_2$ likelihood). The correlation function is evaluated in bins with $\delta r = 4\,h^{-1}$Mpc and $\delta\mu = 0.1$. In these plots bins are ordered first in r (covering $r = 102\,h^{-1}$Mpc to $r = 114\,h^{-1}$Mpc), then in μ ($\mu = 0$ to $\mu = 1$). The difference in the final plot shows that fitting has removed the residuals found in fig. 4, so that the non-Gaussian model precision matrix is now in excellent agreement with the mock precision matrix.

In order to better understand how this fitting works, we expand around a solution $\Psi_{\rm NG} \to \Psi_{\rm NG} + \delta\Psi_{\rm NG}$, finding

$$\delta\left[-\log\mathcal{L}_1\right] = \frac{N_{\rm mocks}}{2}\left[\mathrm{tr}\left(\delta\Psi_{\rm NG}C_{\rm mocks}\right) - \log\det\left(1 + C_{\rm NG}\delta\Psi_{\rm NG}\right)\right] \tag{4.4}$$

$$\approx \frac{N_{\rm mocks}}{2}\mathrm{tr}\left[\delta\Psi_{\rm NG}\left(C_{\rm mocks} - C_{\rm NG}\right)\right], \tag{4.5}$$

so that the likelihood $\mathcal{L}_1$ is maximized when $C_{\rm mocks} = C_{\rm NG}$.

The principal benefit of the likelihood $\mathcal{L}_1$ is that it does not require that we invert $C_{\rm mocks}$. Indeed, this likelihood provides effective constraints on a (or other parameters, should we choose to fit a more elaborate model) even when $C_{\rm mocks}$ is degenerate, i.e. when $N_{\rm mocks} < N_{\rm bins}$. Although we will continue to use the full 1,000 QPM mocks in our analysis, a much smaller number would have led to a very similar $\Psi_{\rm NG}$. We anticipate that because this approach alleviates the need to have very large numbers of mock catalogs, it could be useful in a wide variety of cosmological analyses.

4.2 $\mathcal{L}_2$ Likelihood

The $\mathcal{L}_1$ is not the only possible way to fit one covariance matrix to another. If we consider the goal to be comparison of two matrices, a plethora of methods are available. Noting that our goal is not to compare to arbitrary matrices, but instead to compare the two *distributions* described by those matrices, significantly narrows the field. One prominent candidate is the Kullback-Leibler (KL) divergence (Kullback 1951), which for two multivariate normal distributions (with the same means) specified by Ψ_a and C_b simplifies to

$$KL\left(\Psi_a, C_b\right) = \mathrm{tr}\left(\Psi_a C_b\right) - \log\det\Psi_a - \log\det C_b - N_{\rm bins}\,. \tag{4.6}$$

Note that if we take $\Psi_a = \Psi_{\rm NG}\left(a\right)$ and $C_b = C_{\rm mocks}$, the result is proportional to (4.3), so that we have arrived back at the $\mathcal{L}_1$ likelihood.

The KL divergence is notoriously non-symmetric, so that $KL\left(\Psi_a, C_b\right) \neq KL\left(\Psi_b, C_a\right)$. We can therefore formulate a second likelihood,

$$-\log\mathcal{L}_2\left(a\right) = KL\left(\Psi_{\rm mocks}, C_{\rm NG}\left(a\right)\right), \tag{4.7}$$

which will lead to a slightly different maximum likelihood value for a. Varying this likelihood as above, we find

$$\delta\left[-\log\mathcal{L}_2\right] = \mathrm{tr}\left[\delta C_{\rm NG}\left(\Psi_{\rm mocks} - \Psi_{\rm NG}\right)\right], \tag{4.8}$$

so that where $\mathcal{L}_1$ required agreement between $C_{\rm mocks}$ and $C_{\rm NG}$, $\mathcal{L}_2$ requires agreement between $\Psi_{\rm mocks}$ and $\Psi_{\rm NG}$. While this should not be an issue when the space of distributions spanned by $C_{\rm NG}\left(a\right)$ includes the distribution that gives rise to $C_{\rm mocks}$, when this is *not* the case we cannot expect $\mathcal{L}_1$ and $\mathcal{L}_2$ to yield the same maximum likelihood values. Indeed, by examining fig. 8, which shows the residuals between the mocks and the model precision matrixes, we can see that the $\mathcal{L}_1$ leaves significant residuals while $\mathcal{L}_2$ does not.

The principal benefit of the $\mathcal{L}_2$ likelihood is that it produces better agreement between the mock and model precision matrices than the $\mathcal{L}_1$ likelihood, as shown in fig. 8. Note that most (but not all) applications will require the precision matrix, rather than the covariance matrix. The principal drawback is that it requires that we invert $C_{\rm mocks}$, and so requires that $N_{\rm mocks} > N_{\rm bins}$. In our case this requirement is satisfied, and so we prefer the $\mathcal{L}_2$ likelihood. This preference is however slight, as the resulting $\alpha - \epsilon$ error ellipses, shown in fig. 9, are quite similar.

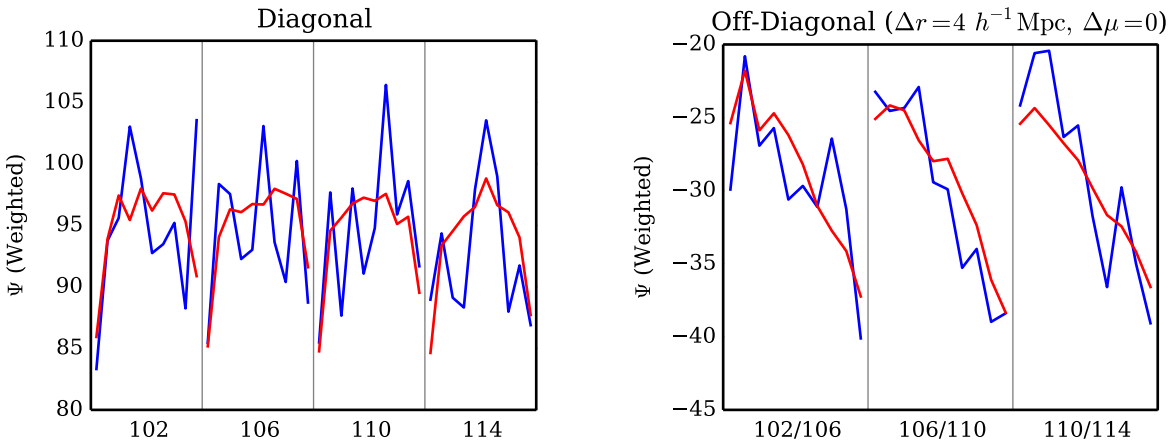

Figure 7. We plot here the most prominent parts of the precision matrices in fig. 6, both from the mocks (blue) and from our non-Gaussian model (red, fit using the $\mathcal{L}_2$ likelihood).

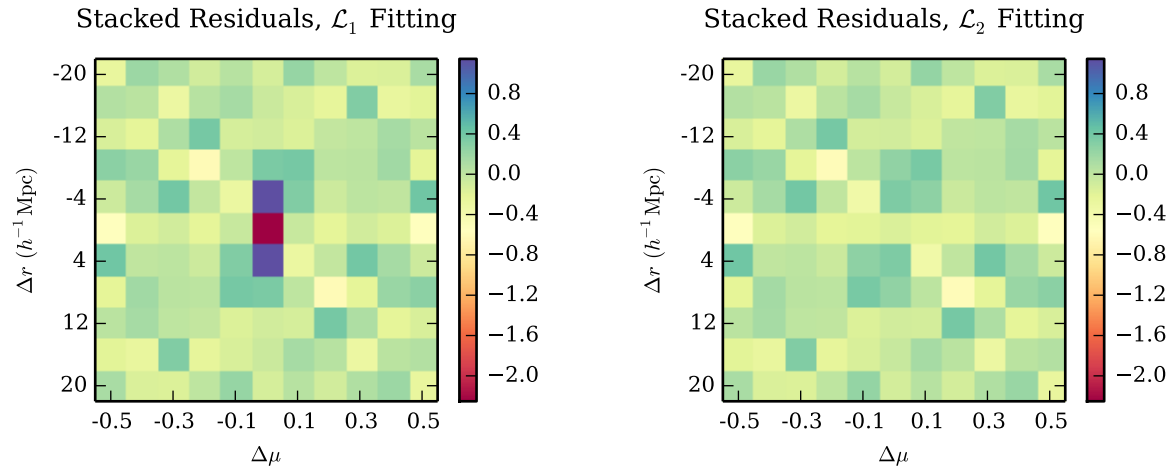

Figure 8. Stacked residuals between our non-Gaussian (fit) models and the mocks. Fitting the non-Gaussian model using the $\mathcal{L}_1$ likelihood significantly reduces the stacked residuals relative to the (unfit) Gaussian model (see fig. 5), while fitting with the $\mathcal{L}_2$ likelihood effectively eliminates the residuals. The absence of residuals indicates that the model precision matrix could replace the mock precision matrix in a variety of applications.

4.3 Results

After using both likelihoods to fit our model to the mock catalogs, we find

$$a_1 = 1.145 \pm 0.002\,, \tag{4.9}$$

$$a_2 = 1.131 \pm 0.005, \tag{4.10}$$

where a_1 is the shot noise rescaling determined using $\mathcal{L}_1$ and a_2 is determined using $\mathcal{L}_2$. We emphasize that this rescaling should not be interpreted as a mismatch between the number density in our code and the actual number density in the mocks, but rather as the additional shot noise required to mimic the effects of short-scale non-Gaussianity for the covariance matrix. The error bars for a_1 and a_2 are determined by jackknife resampling on the mocks, and establish that given 1,000 mocks, the $\mathcal{L}_1$ and $\mathcal{L}_2$ likelihoods do lead to different rescalings of the shot noise.

One way to test the goodness-of-fit of our models is to determine what distribution of the KL divergence would result from noisy realizations of our best-fitting models. In order to ensure that the distributions we generate are comparable to the mocks, we do the following:

(i) Draw 1,000 correlation functions that follow our best-fitting covariance matrix.
(ii) Compute the sample covariance, $C_{\rm noisy}$, and corresponding precision matrix for those draws.
(iii) Fit $C_{\rm noisy}$ or $\Psi_{\rm noisy}$ as appropriate, to generate $C_{\rm refit}$ and $\Psi_{\rm refit}$
(iv) Compute the KL divergence between the $C_{\rm noisy}/\Psi_{\rm noisy}$ and $\Psi_{\rm refit}/C_{\rm refit}$.

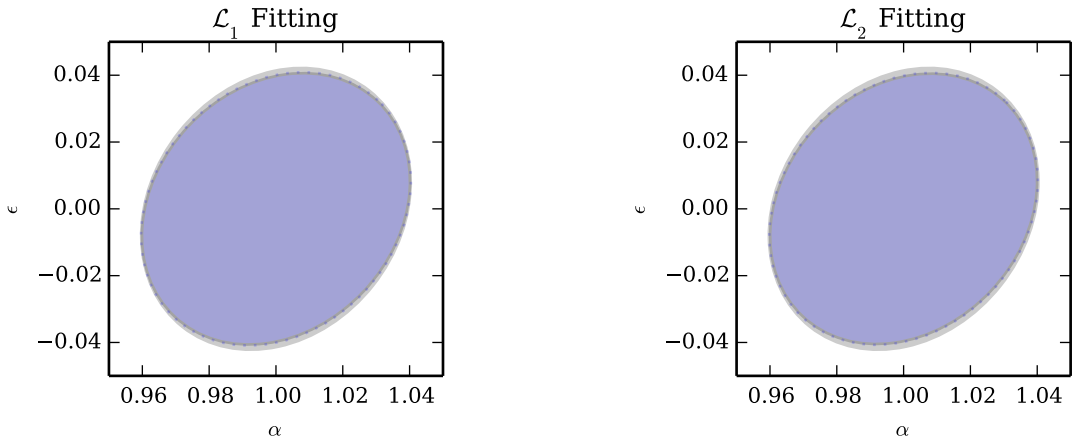

Figure 9. Error ellipses for the BAO parameters α and ϵ from the mocks (gray), the non-Gaussian (fit) models (blue), and noisy realizations of those models (dashed). The discrepancies between the mocks and the Gaussian (fit) model are reduced, though a 3% discrepancy persists in σ_ϵ. The similarity between the two error ellipses indicates that choice of likelihood ($\mathcal{L}_1$ or $\mathcal{L}_2$) for fitting the non-Gaussian model has very little impact on BAO error estimation.

	$C_{\rm test} = C_{\rm mock}$	$C_{\rm test} = C_{\rm noisy}$
$KL\left(\Psi_{\rm G}, C_{\rm test}\right)$	42.14	35.13±0.17
$KL\left(\Psi_{\rm NG}\left(a_1\right), C_{\rm test}\right)$	37.66	35.13±0.17
$KL\left(\Psi_{\rm NG}\left(a_2\right), C_{\rm test}\right)$	37.69	35.13±0.17
$KL\left(\Psi_{\rm test}, C_{\rm G}\right)$	45.76	40.59±0.27
$KL\left(\Psi_{\rm test}, C_{\rm NG}\left(a_1\right)\right)$	42.70	40.59±0.27
$KL\left(\Psi_{\rm test}, C_{\rm NG}\left(a_2\right)\right)$	42.66	40.59±0.27

Table 1. Kullback-Leibler (KL) divergences between our models (Gaussian, and Non-Gaussian fit using $\mathcal{L}_1$ and $\mathcal{L}_2$) and the mock catalogs. In order to calibrate, we have also computed KL divergences between each model and fits to noisy realizations of that model. With 1,000 mocks it is clear that the mock covariance matrix is *not* consistent with noisy realizations of our models.

The results of these tests are collected in table 1. We see that fitting with either likelihood provides a significant improvement over the purely Gaussian model. As anticipated, we find that fitting with the two likelihoods leads to small discrepancies in the resulting KL divergences. We also find that after fitting, the differences between the mock and model covariance matrices are too large to be consistent with noise, indicating that there is room for further improvement in our models.

In order to determine whether our model is sufficient to be used in studies of BAO, we return to the Fisher matrix approach introduced in sec. 3.4. After computing the error ellipses, we would like to know whether the error ellipse from the mocks is consistent with a noisy draw from the model covariance matrix. To determine this we follow a procedure similar to the one described above: we generate sets of 1,000 mock correlation functions drawn following the model covariance matrix, compute the sample covariance for those noisy draws, and then compute the error ellipse from that sample covariance. By repeating this procedure, we can arrive at uncertainties in the uncertainties in α and ϵ, σ_α and σ_ϵ, as well as the uncertainty in their correlation coefficient, $r_{\alpha\epsilon}$. These results are tabulated in table 2. We find that when focusing only on the $\alpha - \epsilon$ error ellipses, and with only 1,000 mocks, the models fit using $\mathcal{L}_1$ and $\mathcal{L}_2$ are indistinguishable, and are consistent at the 1σ level with the QPM mocks. This constitutes an improvement over the unfit Gaussian model, which is $> 2\sigma$ discrepant from the QPM mocks. Thus, while we would be reluctant to use the Gaussian model in some applications, the simple non-Gaussian model introduced here is suitable for use in contemporary BAO studies.

5 OUTLOOK

We have demonstrated that integrating a simple Gaussian model for the covariance matrix of the galaxy correlation function yields a result that is in surprising agreement with that obtained from sample statistics applied to

	σ_α	σ_ϵ	$r_{\alpha\epsilon}$	σ_α (noisy)	σ_ϵ (noisy)	$r_{\alpha\epsilon}$ (noisy)
$C_{\rm mock}$	–	–	–	0.0403	0.0422	0.189
$C_{\rm G}$	0.0384	0.0391	0.216	0.0387±0.0011	0.0394±0.0011	0.217±0.038
$C_{\rm NG}\,(a_1)$	0.0400	0.0405	0.203	0.0403±0.0011	0.0409±0.0012	0.204±0.038
$C_{\rm NG}\,(a_2)$	0.0399	0.0404	0.204	0.0401±0.0011	0.0407±0.0011	0.205±0.038

Table 2. Fisher matrix results for the uncertainties σ_α and σ_ϵ, as well as the correlation coefficient $r_{\alpha\epsilon}$. Even the Gaussian (unfit) model produces reasonable agreement in these parameters, and the level of agreement improves for the non-Gaussian (fit) models. When we restrict our attention to the BAO parameters, we find that the mock precision matrix *is* consistent with a noisy realization of our fit models, at least when we are limited to 1,000 mocks.

mock catalogs. A simple extension of that model, wherein the shot noise is allowed to vary and calibrated against mock catalogs, further improves that agreement, so that for the purposes of BAO measurements the mock and model covariance matrices are statistically consistent with each other. This was accomplished with an effective number of mocks $N_{\rm eff} \sim 35,000$ using just $\approx 1,000$ CPU hours, rather than the hundreds of thousands of CPU hours required to generate and analyse 1,000 QPM mocks. Based on these results, we consider this method of covariance matrix estimation to be a strong alternative to producing very large numbers of mock catalogs. While $\mathcal{O}\,(100)$ mocks will continue to be necessary for estimating systematic errors, we believe those $\mathcal{O}\,(100)$ mocks will be sufficient to calibrate our model, or successors to it. With a reduction in the *number* of mocks required, we anticipate greater effort (both human and computational) can be devoted to improving the *accuracy* of the mocks, ultimately improving the reliability of error estimates from future analyses.

For the sake of simplicity we have focused on reproducing the mock covariance matrix. This is a somewhat artificial goal, since the mock catalogues are themselves imperfect representations of an actual survey. Turning our attention to the survey covariance matrix, we find an opportunity and a challenge. In our method, the mocks are only used to calibrate non-Gaussian corrections, in the form of increased shot noise, to the covariance matrix. Since we expect the effects of non-Gaussianity to be confined to relatively short scales, we can imagine performing this calibration step against simulations with a smaller volume and higher resolution, compared to the mocks. At the same time, we face the challenging question of how to bound possible discrepancies between our model covariance matrix and the true survey covariance matrix. While the accuracy requirements for a covariance matrix (whether derived from mocks or from a model) are ultimately determined by the science goals of a survey, the question of how to determine those requirements and assess whether they have been reached seems largely open.

A clear benefit of mock catalogs is that the same set of mocks can be used for measurement using a variety of observables (e.g. the power spectrum) and cosmological parameters (e.g. $f\sigma_8$, often measured using redshift space distortions). While we have constructed a model covariance matrix suitable for analysis of the galaxy correlation function at BAO scales, our goal of reducing the number of mocks required for future surveys cannot be realized until analogous methods are developed for the other analyses typical of modern surveys. The covariance matrix of the power spectrum has received theoretical attention from many authors (Takahashi et al. 2009, 2011; de Putter et al. 2012; Mohammed & Seljak 2014). Recent efforts (Carron et al. 2014) have come close to presenting a usable model for the covariance matrix of the power spectrum, though the effects of a non-uniform window function have not yet been incorporated. We are optimistic that the necessary extensions of those models can be performed, reducing the required number of mocks for power spectrum analyses to be in line with the $\mathcal{O}\,(100)$ necessary for correlation function analyses.

ACKNOWLEDGEMENTS

RCO is supported by a grant from the Templeton Foundation. DJE is supported by grant DE-SC0013718 from the U.S. Department of Energy. SH is supported by NASA NNH12ZDA001N- EUCLID and NSF AST1412966. NP is supported in part by DOE DE-SC0008080.

Funding for SDSS-III has been provided by the Alfred P. Sloan Foundation, the Participating Institutions, the National Science Foundation, and the U.S. Department of Energy Office of Science. The SDSS-III web site is http://www.sdss3.org/. SDSS-III is managed by the Astrophysical Research Consortium for the Participating Institutions of the SDSS-III Collaboration including the University of Arizona, the Brazilian Participation Group, Brookhaven National Laboratory, Carnegie Mellon University, University of Florida, the French Participation Group, the German Participation Group, Harvard University, the Instituto de Astrofisica de Canarias, the Michigan State/Notre Dame/JINA Participation Group, Johns Hopkins University, Lawrence Berkeley National Laboratory, Max Planck Institute for Astrophysics, Max Planck Institute for Extraterrestrial Physics, New

Mexico State University, New York University, Ohio State University, Pennsylvania State University, University of Portsmouth, Princeton University, the Spanish Participation Group, University of Tokyo, University of Utah, Vanderbilt University, University of Virginia, University of Washington, and Yale University.

This research used resources of the National Energy Research Scientific Computing Center, a DOE Office of Science User Facility supported by the Office of Science of the U.S. Department of Energy under Contract No. DE-AC02-05CH11231.

References

Bernstein G. M., 1994, Astrophysical Journal, 424, 569
Carron J., Wolk M., Szapudi I., 2014, Monthly Notices of the Royal Astronomical Society
Dodelson S., Schneider M. D., 2013, Phys.Rev., D88, 063537
Feldman H. A., Kaiser N., Peacock J. A., 1994, Astrophysical Journal, 426, 23
Kullback S.; Leibler R. A., 1951, Ann. Math. Statist., 22, 79
Laureijs R., et al., 2011, preprint, (arXiv:1110.3193)
Levi M., et al., 2013, preprint (arXiv:1308.0847)
Mohammed I., Seljak U., 2014, Monthly Notices of the Royal Astronomical Society, 445, 3382
Percival W. J., et al., 2014, Monthly Notices of the Royal Astronomical Society, 439, 2531
Spergel D., et al., 2015, preprint, (arXiv:1503.03757)
Swanson M. E., Tegmark M., Hamilton A. J., Hill J. C., 2008, Monthly Notices of the Royal Astronomical Society, 387, 1391
Takahashi R., et al., 2009, Astrophysical Journal, 700, 479
Takahashi R., et al., 2011, Astrophysical Journal, 726, 7
Taylor A., Joachimi B., Kitching T., 2013, Monthly Notices of the Royal Astronomical Society, 432, 1928
White M., Tinker J. L., McBride C. K., 2014, Monthly Notices of the Royal Astronomical Society, 437, 2594
Xu X., Cuesta A. J., Padmanabhan N., Eisenstein D. J., McBride C. K., 2013, Monthly Notices of the Royal Astronomical Society, 431, 2834
Zhu F., Padmanabhan N., White M., 2015, Monthly Notices of the Royal Astronomical Society, 451, 4755
de Putter R., Wagner C., Mena O., Verde L., Percival W. J., 2012, Journal of Cosmology and Astrophysics, 4, 19